The role of BaTiO3 polarization on CO oxidation

Céline Dupont

The role of $BaTiO_3$ polarization on CO oxidation

Céline Dupont*

Laboratoire Interdisciplinaire Carnot de Bourgogne, UMR 6303 CNRS-UBFC, 21078 Dijon Cedex, France

E-mail: celine.dupont@u-bourgogne.fr

Abstract

The influence of polarization on the probe reaction CO oxidation is studied thanks to DFT calculations. Following recent experimental results and common behaviors on metal oxides, a Mars-Van Krevelen mechanism is adopted. The adsorption of CO is thus firstly studied, illustrating both the role of polarization and the one of termination. While P_{up} TiO_2 termination presents the most favorable interaction with CO, allowing a spontaneous oxidation in CO_2, an activation barrier has to be overcome on P_{down} domain. Given the ability of $BaTiO_3$ for CO oxidation, desorption of CO_2 appears as the rate determining step on both terminations, but again polarization can be used to go over this issue. Finally, recovery of $BaTiO_3$ slab through O_2 dissociation also behaves diversely depending on the termination and on the polarization. Through this study we thus demonstrated the key role of polarization to improve CO oxidation.

Introduction

Ferroelectric compounds, and especially the non-toxic $BaTiO_3$ (BTO), have aroused more and more interest recently, with more than 500 papers per year dealing with BTO these last 5 years. Use of the intrinsic polarization of these compounds can be greatly highlighted in

several applications, like in photoelectrochemical systems for increasing the charge-carriers separation,[1] in energy storage capacitors[2] or in electronic ceramics industry.[3] Ferroelectricity can also play a primary role in catalysis, as exemplified in a recent review.[4] First experimental evidence of the role of ferroelectricity on reactivity has been brought by Parravano in the fifty's.[5] Following this work, several papers have evidenced experimentally or theoretically the influence of polarization on either adsorption[6–13] or reactivity[14,15] of different systems. Conversely, the adsorption can also modify the polarization of a system, as demonstrated both experimentally and theoretically.[16,17] Finally, the idea of using ferroelectricty to improve catalysis by tailoring the reactivity has also been proposed. In particular, one can mention several works dealing with switchable chemistry.[18–22] The aim in these papers is to use ferroelectric supports, mostly $PbTiO_3$, to modify catalytic properties of the capping system by switching from up to down (or the other way around) polarization, depending on which is the most favorable for the considered step. If this concept appears as very interesting and promising, most of the examples mentioned above deal with $PbTiO_3$, certainly due to its high intrinsic polarization, but its toxicity related to the presence of lead prevents sustainable applications of this compound. On the contrary, very few studies about polarization influence on reactivity have been devoted to the non-toxic $BaTiO_3$.[23–25] In particular, the influence of $BaTiO_3$ polarization on CO oxidation has been barely investigated. As far as we know, the only study on this subject is the one of Piccolo and coworkers[23] which demonstrates that CO oxidation on $BaTiO_3$ (poled Up - TiO_2 terminated) occurs through a Mars-Van Krevelen mechanism. Given the importance of CO oxidation, being both a probe reaction and a reaction of interest for numerous applications (in green chemistry, fuel cells ...) and the potential interest of ferroelectricity to improve catalysis, it appears of prime interest to perform an in-depth study of the influence of $BaTiO_3$ polarization on CO oxidation.

In this paper, we use Density Functional Theory (DFT) to investigate in details the role of BTO polarization, first on CO adsorption, then on CO oxidation itself.

Computational Details

Density Functional Theory (DFT) calculations were performed using the Vienna *ab initio* simulation package VASP code,[26,27] with a plane-wave energy cutoff of 500 eV. The projector augmented wave (PAW) potentials were used to describe the electron-ion interaction,[28,29] with explicitly included ten valence electrons for Ba ($5s^2$ $5p^6$ $6s^2$), six for O ($2s^2$ $2p^4$), twelve for Ti ($3s^2$ $3p^6$ $4s^2$ $3d^2$) and four for C ($2s^2$ $2p^2$). The generalized gradient approximation (GGA) was employed with Perdew-Burke-Ernzerhof (PBE)[30] exchange correlation functional. As it is well known that DFT has issues to properly describe the strong correlation between d electrons, the DFT+U approach was used by including an on-site Coulomb repulsion U-term for the Ti $3d$ electrons, adopting the Dudarev method.[31] In agreement with our previous study,[32] a value of U_{eff}=3.5 eV was applied, leading to a band gap of 2.23 eV. Following our previous work,[32] reference values of $a = 4.006$ Å and $c = 4.184$ Å were taken for lattice parameters of BTO unit cell, leading to a c/a ratio of 1.044. BTO was modeled with a slab of 11 layers with atoms allowed to relax. As BTO is often used deposited on platinum substrate, the 2.1% lattice mismatch induced by the 3.92 Å experimental lattice parameter of platinum is taken into account. Nevertheless, apart from geometric influence induced by the strain, the presence of platinum has not any electronic influence on CO adsorption on BTO. Thus in the following, platinum is not explicitly considered to reduce computational cost. Besides, we follow the approach of Migoni[33] to model the out-of-plane polarization. In short, the slab is divided into two domains of opposite polarization, leading to an overall cell with no net dipole moment. As a consequence and to clearly distinguish area of adsorption on positive and negative domains, a large supercell of 31.36 Å$\times$ 7.84 Å was used. Finally, a 20 Å vacuum was considered to separate periodic images along the z direction.

The convergence threshold on total energy was set to 10^{-6} eV, while structural optimization was stopped when the forces converged below 0.01 eV/Å. Given the size of the unit cell, calculations were performed at gamma point, with a Gaussian smearing of 0.20 eV.

For the modelling of reaction pathways and the search of transition states, the Climbing-Image Nudged Elastic Band (CINEB) method[34] was used. Each transition state was then characterized by vibrational analysis.

Results and discussion

CO adsorption

Prior to any study of reactivity, the adsorption of the main reactant, namely CO, is considered on BTO. Given our previous results,[32] when grown of platinum, both top TiO_2 and BaO terminations are competitive and will thus be considered in the following. For each system, adsorption of CO is considered on the paraelectric phase and on the ferroelectric one. For the latter case, CO is put either on the domain with polarization up or on the one with polarization down or at the frontier between these two domains. For all cases, standard initial adsorption states, namely top, bridge and hollow sites, have been investigated, with systematically considering different relative distance towards the frontier of the polarization domain. All possible cases are thus reported in Figure 1, as well as the initial values of local polarization, calculated with the formula developed by Vanderbilt[35] and applied as explained in ref.[32,36] Besides, in this study, only out-of-plane polarization will be discussed, as both polarizations in the [010] and [100] directions are not or slightly impacted by considered phenomena. As can be seen on top view of Figure 1, prior adsorption, polarization is similar for cells at the front or in the back along the [010] direction, hence on side view only polarization for cells at the front is reported. Finally, as observed on this side view, polarization patterns along the [001] direction are in agreement with the ones already calculated.[32]

Adsorption on TiO_2 termination

The adsorption of CO is firstly considered on the paraelectric TiO_2 termination. However, whatever the initial position of CO on the paraelectric phase, it always leads to a polarization

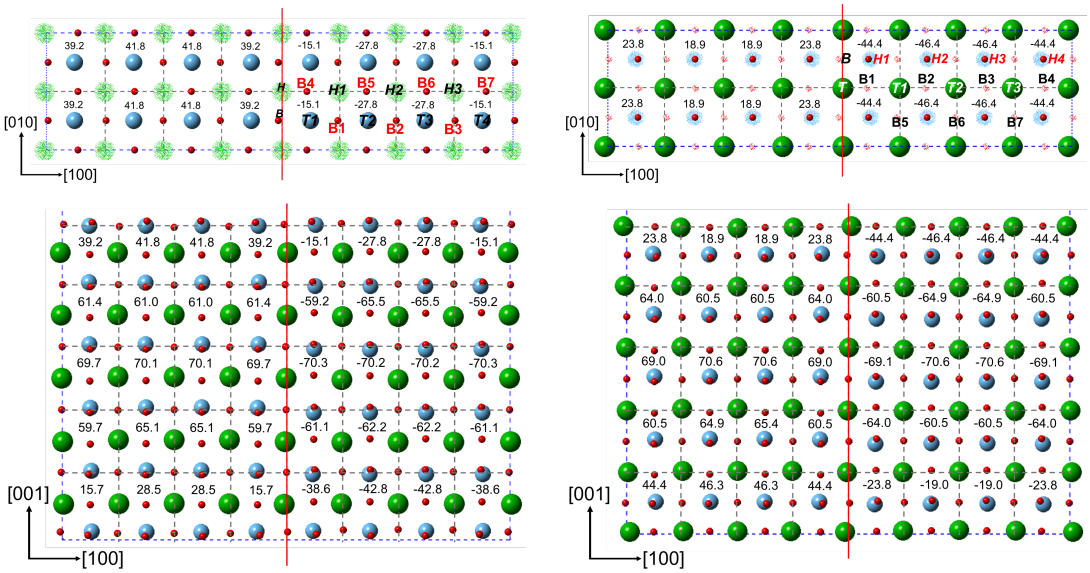

Figure 1: (Top) Top and (Bottom) Side views of (Left) TiO_2 and (Right) BaO terminated slabs. The red line indicates the frontier between the half of the slab polarized up (left) or the one polarized down (right). Dotted lines delimit reference cells used for calculating local polarization. Values in each cell indicate the local polarization (in $\mu C/cm^2$). Initial positions for CO adsorption are reported (only on part polarized down for the sake of clarity), with the following labels: T stands for Top, B for Bridge and H for Hollow. Associated numbers allow to distinguish the different possibilities for each site. Barium atoms are reported in green, Ti in blue, and oxygen in red.

of the slab. In the following we will thus focus only on ferroelectric systems, with adsorption energies reported in Table 1.

Table 1: Adsorption energies in eV for CO adsorbed on TiO_2 termination, calculated with respect to gas phase CO. Results for both polarizations are reported. Labels are those defined in Figure 1. For unstable cases, label of obtained final state is reported, while X refers to CO desorption.

	E_{ads} (eV)	
Sites	Polarization Down	Polarization Up
T1	-0.38	-0.50
T2	-0.34	-0.53
B1	T2	T1
B2	T2	T2
B4	-0.01	-0.23
B5	-0.01	-2.03
H1	T1	X
H2	X	X
H3	T4	T3

Before discussing in details these results, the case of adsorption at the frontier of the two domains of opposite polarizations should be mentioned. As reported in Figure 1, adsorption either on a bridge or on a hollow site at the frontier has been considered. These structures are not reported in Table 1 as they evolve in already studied cases, namely T1 of P_{down} domain and T1 of P_{up} one, respectively.

Concerning P_{down} domain, most of the explored cases on this polarization do not stabilize in their initial position. Firstly, bridge sites along the [010] direction (B1 and B2) evolve on a neighbouring top site. At the same time, bridge sites along the [100] direction (B4 and B5) lead to a pseudo-bridge position between Ti and O (see SI for corresponding structure), however this configuration is not competitive with an almost null adsorption energy (-0.01 eV). Additionally none of the hollow sites is stable, H1 and H3 evolve on a top site, while H2 desorbs. Finally, only top sites need to be investigated in details. T1 and T2 differ by their position in the P_{down} domain: T1 being close to the limit with the P_{up} domain, while T2 is in the middle of the P_{down} one. These sites present slightly different adsorption energies of -0.38 and -0.34 eV, respectively. The obtained structures and corresponding polarization are

reported in Figure 2. For the sake of clarity, only the front cells of the first five layers are described, while the whole cell is reported in SI. Given the calculated values, the presence

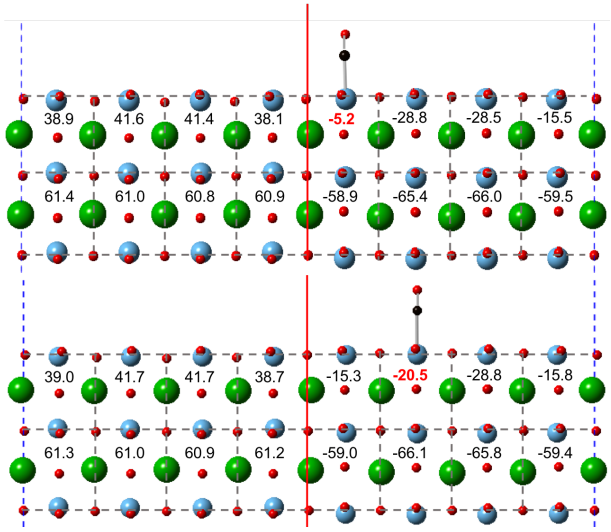

Figure 2: Side views of CO adsorption on (Top) T1 and (Bottom) T2 sites on P_{down} domain of TiO_2 termination. Only front cells of the first five layers are represented, while the whole cell is reported in SI. Values in each cell correspond to the local polarization in $\mu C/cm^2$. Barium atoms are reported in green, Ti in blue, O in red and C in black. Same colors will be used in all figures.

of CO affects the polarization only locally. Indeed, only the cell on which CO is adsorbed presents a significant modification of its polarization, from -15.1 to -5.2 $\mu C/cm^2$ for T1 and from -27.8 to -20.5 $\mu C/cm^2$ for T2. For both cases, this evolution directly comes from the relaxation of the titanium atom on which CO is adsorbed. Indeed, the presence of CO induces an outward relaxation of Ti of 0.05 Å for T1 and 0.07 Å for T2.

Concerning now P_{up} domain, as for P_{down} side, several of the initial cases evolve in a different stable position. First of all, hollow sites desorb and thus will not be discussed. On the contrary, all optimized top sites are stable, with similar adsorption energies of -0.50 and -0.53 eV, depending on the relative position towards the frontier with P_{down} domain. Contrary to what occurs on domain polarized down, here T2 site in the middle of the P_{up} domain is slightly more stable (-0.53 eV) than T1 (-0.50 eV) at the border. According to values reported in Figure 3, the presence of CO leads mainly, like on P_{down} domain, to an increase of polarization of the cell on which CO is adsorbed, surrounding cells being far less affected.

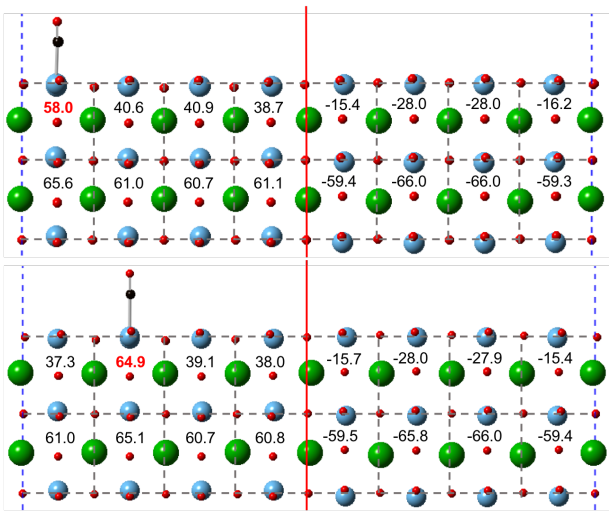

Figure 3: Side views of CO adsorption on (Top) T1 and (Bottom) T2 sites of P_{up} domain of TiO_2 termination. Only front cells of the first five layers are represented, while the whole cell is reported in SI. Values in each cell correspond to the local polarization in $\mu C/cm^2$.

This increase is larger than the one observed for the P_{down} domain: local polarization evolves from 39.2 to 58.0 $\mu C/cm^2$ for T1 site and to 64.9 $\mu C/cm^2$ for T2. This higher increase can be explained by an initial favorable orientation. Indeed, as for P_{down} domain, the increase of polarization is predominantly related to the displacement of Ti atom bonded to CO, with a relaxation of 0.11 and 0.14 Å for T1 and T2, respectively. But contrary to P_{down} domain where adsorption of CO has to counter initial orientation of Ti, here both CO adsorption and initial polarization act in the same direction. This synergy explains the larger adsorption energy and the higher increase of polarization observed on the P_{up} domain. Finally, for bridge sites, several behaviors can be observed. Sites along [100] (B1, B2) evolve on top positions on cells at the frontier with the P_{down} domain. In the meantime, B4 evolves in a pseudo-bridge position between Ti and O (see SI for corresponding structure), being less stable than top sites with E_{ads} = -0.23 eV. Besides, given the particularity of this site, the symmetric position (B7) has also be optimized and evolves to T1. Thus, the pseudo bridge position obtained through B4 optimization is certainly a metastable intermediate before reaching the stable T1 position and will not be considered in the following. Finally, the last case corresponds to B5 along [010], reported in Figure 4. According to Table 1, adsorption

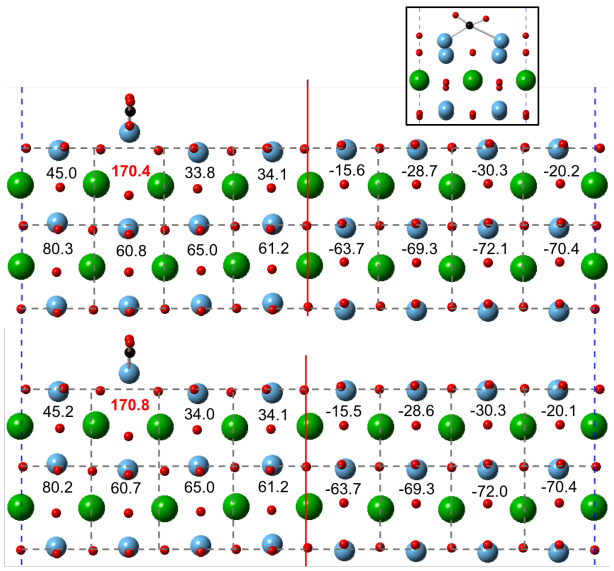

Figure 4: Side views of CO adsorption on B5 site of P_{up} domain of TiO_2 termination. (Bottom) Back cells, (Top) front cells and in insert, view of adsorbed CO along [100] direction are reported. Only the first five layers are represented, while the whole cell is reported in SI. Values in each cell correspond to the local polarization in $\mu C/cm^2$.

on this bridge site is by far the most stable with E_{ads} = -2.03 eV. As can be seen in Figure 4, this stability comes from the spontaneous formation of CO_2, by creation of a bond between CO and a bridging oxygen from the BTO lattice, along [010] direction. Final structure presents two CO bonds of 1.29 and 1.30 Å, consistent with elongation of C-O bond induced by adsorption, compared to gas phase CO_2 (d_{CO} = 1.16 Å). Adsorption of this CO_2 induces an extraction of the two related Ti atoms by almost 1 Å. This has a direct consequence on the polarization of the two underneath cells, which climbs from 41.8 to 170.4 $\mu C/cm^2$ (and 170.8 $\mu C/cm^2$). Surrounding atoms and thus associated polarizations are also affected, but in a lesser extent.

Adsorption on BaO termination

As for TiO_2 termination, all sites described in Figure 1 have been screened, with obtained adsorption energies summarized in Table 2. Adsorption on paraelectric slab also leads to polarization of the system, and thus will not be discussed in itself. First of all, contrary to TiO_2 termination, none of the top sites is stable on the P_{down} domain, they all lead

Table 2: Adsorption energies in eV for CO adsorbed on BaO termination calculated with respect to gas phase CO. Results for both polarizations, as well as for adsorption at the frontier between the two domains, are reported. Labels are defined in Figure 1.

	E_{ads} (eV)		
Sites	Polarization Down	Polarization Up	Frontier
T1	X	-0.14	-0.10
T2	X	-0.16	-
T3	X	-0.14	-
B1	H1	-0.13	-0.90
B2	H2	-0.15	-
B5	H2	-0.14	-
B6	H2	-0.16	-
H1	-0.91	-0.12	-
H2	-1.10	-0.16	-

to desorption with d(Ba-C) $>$ 3.4 Å. CO on bridge sites is also not stable and evolves to hollow sites. Finally both types of hollow sites are stable with different behaviors depending on initial local polarization. Indeed, H1 is less stable (-0.91 eV) than H2 (-1.10 eV). This latter is in the middle of the P_{down} domain, with slightly higher initial local polarization in absolute value (-46.4 instead of -44.4 μC/cm^2). Obtained geometries and local polarizations are reported in Figure 5. First of all, one can observe that CO does not adsorb linearly like on the TiO_2 termination, but it adopts a tilted geometry, even more pronounced for H1 than for H2. In both cases, a new C-O bond is created between the carbon atom of adsorbed CO and an oxygen atom from the BTO lattice, leading to an extraction of this O from the surface. Indeed, while on polarized bare slab, lattice O is almost in the same plane than surrounding Ba atoms (Δz = 0.01 Å), after CO adsorption, Δz for H1 and H2 evolves to 0.28 and 0.81 Å, respectively. In agreement, the new C-O bond is shorter for H2 than H1 (1.33 instead of 1.37 Å), associated with a higher adsorption energy (-1.10 compared to -0.91 eV). Accordingly, local polarization is greatly increased, from -44.4 and -46.4 μC/cm^2 for respective underneath cells of H1 and H2 before adsorption, to -119.9 and -209.9 μC/cm^2 after CO adsorption on H1 and H2, respectively. If one of the main reasons is the extraction of surface O already discussed, other phenomena act in synergy. In particular, while presence

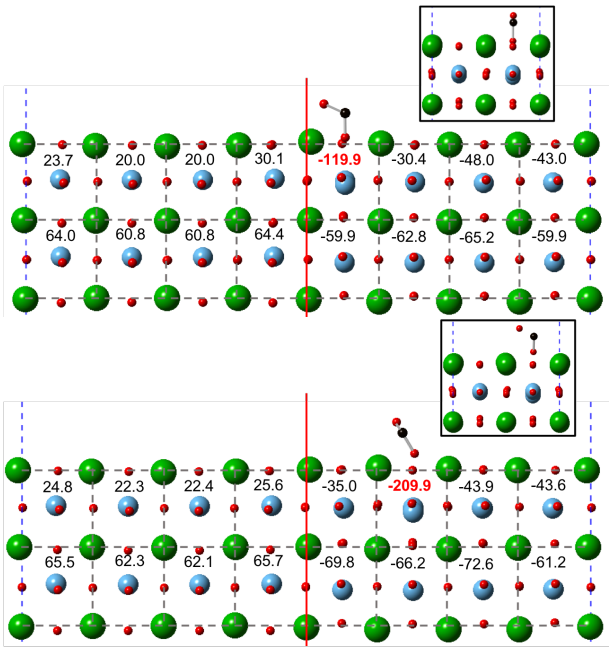

Figure 5: Side views of CO adsorption on (Top) H1 and (Bottom) H2 sites on P_{down} domain of BaO termination. Insert reports a lateral view along [100] direction. Only front cells of the first five layers are represented, while the whole cell is reported in SI. Values in each cell correspond to the local polarization in $\mu C/cm^2$.

of CO extracts surface O, it pushes the underlying Ti. As a consequence, the Ti-O bond increases from 2.12 Å in the bare slab to 2.63 Å after CO adsorption on H1 and even 3.23 Å after adsorption on H2. This evolution in itself is to a considerable extent responsible for the increase of local polarization, but additionally it is reinforced by a climbing of oxygen atoms of the TiO_2 layer.

Concerning P_{up} domain, results are not as straightforward. First of all, as reported in Table 2, all adsorption energies are very close with values between -0.12 and -0.16 eV. In all cases, CO stands far from the surface with d(Ba-C) always higher than 3.30 Å, confirming a very weak interaction. As can be seen in Figure 6, CO remains straight for top position, while it is tilted for bridge and hollow positions. According to Figure 6, both cells of the front part (as well as both of the back part, see SI) below CO present a small increase of their local polarization. This can be attributed to electrostatic interactions of CO with the surface. This is consistent with well-known behavior of CO on other oxide surfaces like MgO, as

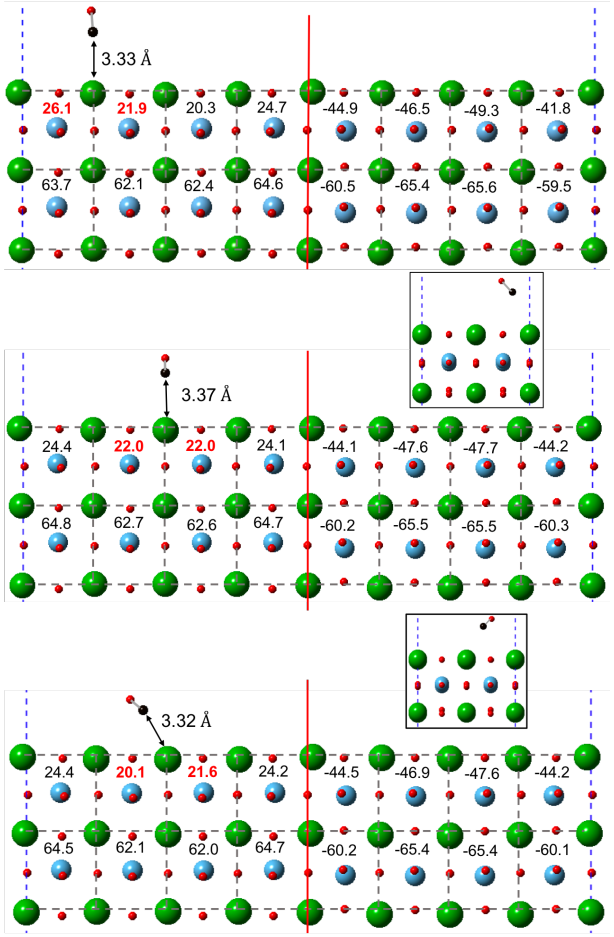

Figure 6: Side views of CO adsorption on T1, B6 and H2 on P_{up} domain of BaO termination. For B6 and H2, insert reports a lateral view along [100] direction. Only front cells of the first five layers are represented, while the whole cell is reported in SI. Values in each cell correspond to the local polarization in $\mu C/cm^2$.

already reported by Sauer *et al.*[37] This change in polarization plays certainly the main role in the small adsorption energies.

Finally, the case of adsorption at the frontier between P_{up} and P_{down} domains is analyzed. The adsorption on top site is similar than for top sites of the P_{up} domain, with d(Ba-C) even larger (3.41 Å) leading to a weaker adsorption energy of -0.10 eV. Thus this case will not be discussed in the following. Bridge site also does not stay at the frontier, but evolves towards the P_{down} domain, the optimized state is reported in Figure 7. According to both

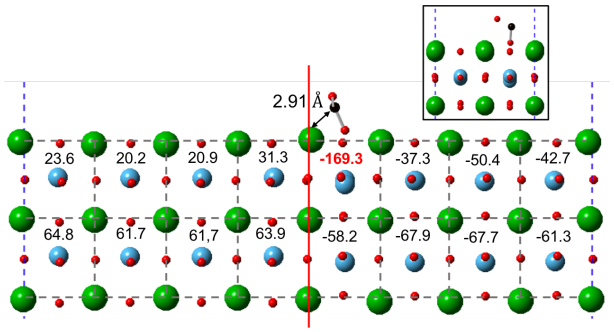

Figure 7: Side view of CO initially adsorbed on a bridge site at the frontier of both domains on BaO termination. Insert reports a lateral view along [100] direction. Only front cells of the first five layers are represented, while the whole cell is reported in SI. Values in each cell correspond to the local polarization in $\mu C/cm^2$.

adsorption energy (-0.90 eV) and general geometry, this structure looks very close to CO adsorption on H1 site of P_{down} domain (see Figure 5). Nevertheless some discrepancies occur leading in particular to a higher increase of polarization, final polarization being equal to -169.3 $\mu C/cm^2$, instead of -119.9 $\mu C/cm^2$ for H1 on P_{down} domain. Main difference comes from the orientation of the CO molecule, inducing a higher extraction of the lattice oxygen in the current case, compared to CO intially adsorbed on H1. Indeed, here Δz(Ba-O) is equal to 0.59 Å, while it was only of 0.28 Å with initial adsorption on H1. One can note that this value of 0.59 Å is intermediate between values obtained on H1 and H2 (0.28 and 0.81 Å, respectively), in agreement with an intermediate local polarization: -169.3 $\mu C/cm^2$, compared to -119.9 and -209.9 $\mu C/cm^2$ for H1 and H2, respectively.

Reaction pathways

CO oxidation

Following previous experimental results[23] and in agreement to what mostly happens on oxides, we consider that CO oxidation occurs through a Mars-van Krevelen mechanism. In this framework, the first step to be considered is the extraction of a lattice oxygen by the adsorbed CO. According to the adsorption study, two cases will be considered on the TiO_2 termination, namely oxidation from CO adsorbed on T1 on P_{down} domain and on B5 on P_{up} domain. Concerning BaO termination, we will investigate oxidation from CO adsorbed on H2 on either P_{down} or P_{up} domain.

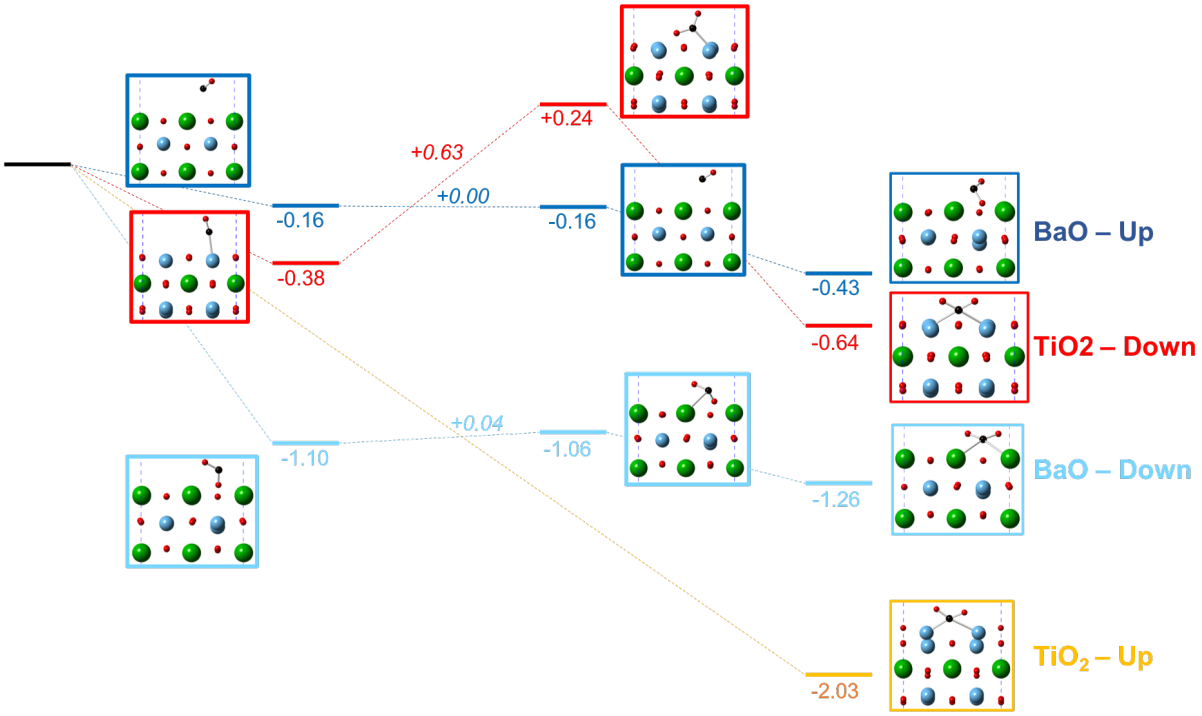

Figure 8: CO oxidation pathways on the four selected models: (Red) TiO_2 - Down; (Orange) TiO_2 - Up; (Dark blue) BaO - Up; (Light blue) BaO - Down. All energies are reported in eV, with bare polarized slab and gas phase CO as references. Lateral views along the [100] direction are reported for all initial, transition and final states.

According to Figure 8 and in agreement with CO adsorption results, CO oxidation on P_{up} domain of TiO_2 is by far the most efficient pathway, from both thermodynamic and kinetic points of view. Indeed on this termination, formation of CO_2 is exothermic by 2.03 eV and

occurs without activation energy. This spontaneous and highly exothermic formation of CO_2 with a lattice oxygen atom supports previous experimental results[23] demonstrating that CO oxidation occurs through a Mars-Van Krevelen mechanism. The situation completely differs on the P_{down} domain, where CO oxidation is now exothermic by only 0.25 eV and most importantly an activation energy barrier of +0.63 eV is required to oxidize CO. The difference of exothermicity can be directly attributed to the difference of polarization. Actually, the synergetic effect between polarization and extraction of surface Ti atoms due to CO_2 adsorption explains the larger stabilization observed for CO_2 on P_{up} domain compared to P_{down} one.

These results can be compared with previous studies about CO oxidation on TiO_2. In particular, Pacchioni and coworkers[38] have demonstrated the improvement of CO oxidation on TiO_2 by the presence of a gold nanoparticle. Indeed, while on anatase CO oxidation is endothermic by more than 1.3 eV (so an expected barrier even higher), they obtained an athermic oxidation on Au/TiO_2 with an activation barrier of 0.97 eV. Here we demonstrate that the presence of polarization or that of the BaO sublayer or both allows to improve again CO oxidation on TiO_2. Indeed, both cases studied here lead to an exothermic oxidation, with the highest barrier being of only 0.63 eV.

Concerning the BaO termination, both possible paths are exothermic with ΔE = -0.27 and -0.16 eV, for P_{up} and P_{down} domain, respectively. Besides, we calculated a null activation energy barrier for P_{up} domain and one that can be neglected (+0.04 eV) for P_{down} one. These two paths thus only differ by the thermodynamic aspect. From this point, even if P_{down} domain has a lower exothermicity, it appears as preferential with a stabilization of the final state by -1.26 eV compared to -0.43 eV on P_{up} domain. This is in agreement with the geometries of final states. Indeed, while CO_2 has almost its gas phase structure on P_{down} domain with both C-O bonds equal to 1.28 Å, its formation is not as advanced on P_{up} domain with in particular $d(C\text{-}O_{latt})$ = 1.37 Å. This can be directly related to the ability of the slab to form oxygen vacancies. To confirm this point, we calculated the cost to create a

vacancy on each domain, considering gas phase O_2 as a reference. We thus evidenced that the creation of a vacancy costs 3.78 eV on the P_{down} domain, while this price climbs to 5.55 eV on the P_{up} domain. Thus contrary to TiO_2 termination, CO oxidation is favored on the P_{down} domain for BaO termination.

Finally, CO_2 desorption has to be mentioned. At the end of both paths, CO_2 is strongly adsorbed, leading to a rather important cost for desorption. Even if this strong adsorption is consistent with previous results,[38–40] one can take advantage of polarization to overcome this cost. In particular, we calculated how CO_2 adsorption evolves when polarization is reversed while keeping same adsorption positions. So we demonstrated that on TiO_2 termination adsorption energy of CO_2 weakens from -2.02 to -0.22 eV when polarization is switched from up to down while on BaO it evolves from -1.26 to -0.51 eV. Hence in both cases, inversion of polarization can be used to facilitate CO_2 desorption. This can be achieved by introducing an electric field like it has already been done using Piezoresponse Force Microscopy (PFM).[41]

O_2 dissociation

Once CO_2 has been formed creating a vacancy on BTO, an oxygen molecule is added to fill this vacancy and thus recover initial slab with an adsorbed atomic oxygen. Obtained pathways are reported in Figure 9. For each case, the reference is the slab with a vacancy in the position corresponding to CO_2 formation for this domain and gas phase O_2. First of all, one can observe that whatever the termination or the polarization, O_2 adsorption is widely favored on incomplete $BaTiO_3$, with adsorption energies between -4.06 and -5.77 eV. Nevertheless, adsorption on P_{up} domains is systematically more stable than on P_{down} ones. Starting from these initial states, O_2 dissociation appears to be exothermic only on the TiO_2 termination, with similar ΔE of -0.26 and -0.21 eV on P_{down} and P_{up} domains, respectively. On the contrary, both polarizations of BaO termination lead to endothermic dissociation. While it is rather limited on the P_{up} domain ($\Delta E = 0.12$ eV), the dissociation is widely endothermic on the P_{down} domain with $\Delta E = 2.15$ eV, with a very late transition state

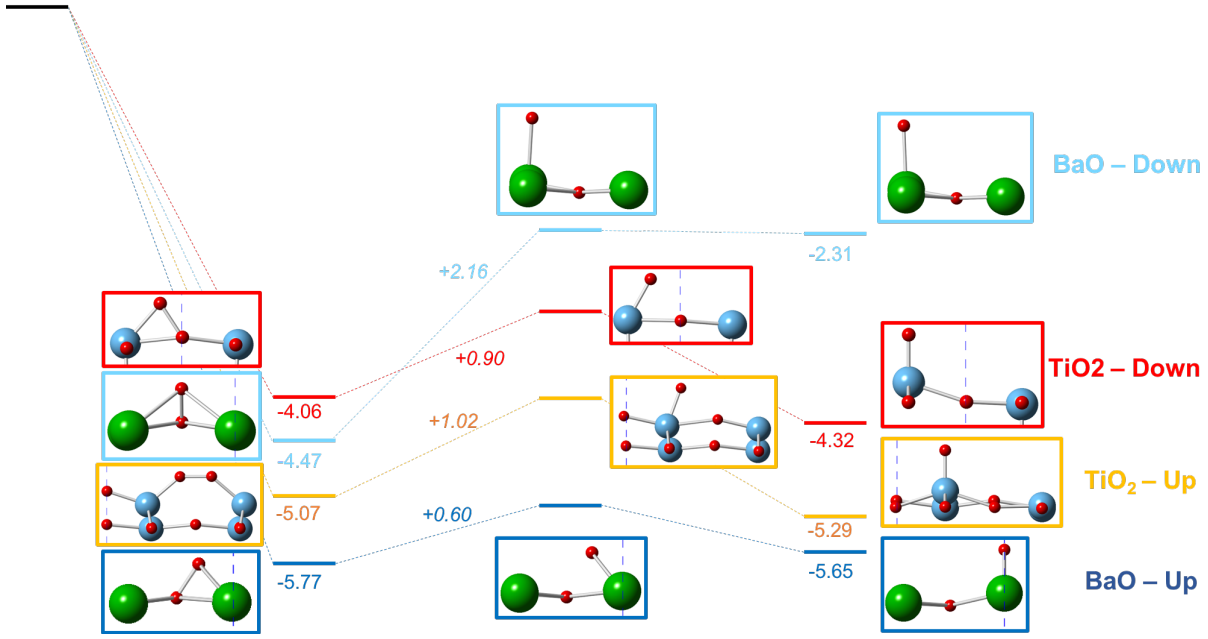

Figure 9: O_2 dissociation pathways on the four selected models: (Red) TiO_2 - Down; (Orange) TiO_2 - Up; (Dark blue) BaO - Up; (Light blue) BaO - Down. All energies are reported in eV, with bare polarized slab with a vacancy (from CO oxidation) and gas phase O_2 as references. Lateral views along the [100] direction are reported for all initial, transition and final states. For the sake of clarity, only closest neighbours of active site are reported.

associated to a large activation energy of 2.16 eV. One can thus exclude O_2 dissociation and thus recovery of complete slab on BaO with down polarization. This difference of behavior can be explained by the geometry of the final state. Indeed on the P_{down} domain, atomic oxygen is adsorbed on top of a Ba atom, while it is on a bridge position on the P_{up} domain, leading to two Ba-O bonds and thus a higher stabilization.

On TiO_2, despite the wide geometrical differences, both polarizations present similar energetic behaviors. First of all, on both sides dissociation is exothermic with reaction energies of -0.26 and -0.21 eV on P_{down} and P_{up} domains, respectively. Activation energies are also of the same order of magnitude with values of 0.90 and 1.02 eV on P_{down} and P_{up} domains, respectively. The difference in activation energies comes directly from the geometries. On the P_{down} domain, the vacancy is easily reachable, allowing O_2 to adsorb in a position that almost already recovers original slab. As a consequence the elongation of the O-O bond (d(O-O) = 1.47 Å) after adsorption is rather significant. On the contrary, the

large relaxation of Ti atoms around the vacancy on P_{up} domain, makes harder the access to the vacancy. In this case, none of the oxygen atoms of O_2 can reach a position that directly fills the vacancy. The initial state is thus farther leading to a higher transition state. Finally, final states present similar geometries with atomic O adsorbed on top of a Ti atom. The higher stability observed on P_{up} domain is directly related to the polarization direction acting in synergy with the effect of adsorbed O.

As for CO oxidation, our results can be compared with previous studies. In particular, reoxidation of TiO_2 after CO oxidation has been considered in presence of supported Au[38] or supported Pt[39] on TiO_2. In both cases, the full process is widely exothermic with a ΔE of -5.09 eV for Au/TiO_2 and -4.32 eV for Pt_4/TiO_2, values thus being in the same range than the ones we obtained on both terminations of BTO. Results are also consistent for activation energies with barriers of 0.94 and 0.74 eV on Au/TiO_2 and Pt_4/TiO_2, respectively. These values can be directly compared with our values of 1.02 and 0.60 eV for TiO_2 and BaO termination, respectively.

Finally, last step corresponds to the recovery of the initial $BaTiO_3$ slab through the oxidation of a second CO molecule. This final step will not be described in detail, as for all cases, interaction of this new CO molecule with the "$BaTiO_3$ - O" slab leads to a spontaneous exothermic formation of CO_2.

Conclusions

In order to analyze the influence of polarization on CO oxidation, CO adsorption and consecutive reaction have been investigated in detail on both terminations of ferroelectric $BaTiO_3$. Firstly, CO adsorption clearly presents different behaviors depending on the considered termination or polarization. While on TiO_2 termination adsorption is stronger on P_{up} domain thanks to a synergetic influence of polarization and bonds' formation, CO adsorbs preferentially on P_{down} domain on BaO termination. Preferential sites also differ with top and bridge

being more stable on TiO_2 termination and hollow preferred on BaO one.

On TiO_2 with polarization up, CO adsorption leads directly to its oxidation in CO_2 with no barrier. Once adsorbed on BaO termination, CO oxidation will occur with no or insignificant barrier, depending on the polarization. Finally, only TiO_2 with polarization down presents an activation energy of 0.63 eV.

On the other hand, second step of O_2 dissociation presents different behaviors on both terminations. While all polarizations lead to exothermic reaction on TiO_2 termination, O_2 dissociation is endothermic on BaO one, being even almost impossible with P_{down} polarization.

In summary, on ferroelectric $BaTiO_3$, CO oxidation will occur through a Mars-Van Krevelen mechanism, on P_{up} domains, preferentially on TiO_2 termination than on BaO one. Besides, whatever the polarization the presence of underneath BaO layers or the one of polarization or both allows to facilitate CO oxidation on TiO_2 termination compared to pristine or supported TiO_2.

Acknowledgement

Calculations were performed using HPC resources from DNUM CCUB (Centre de Calcul de l'Université de Bourgogne). This work was also granted access to the HPC resources of IDRIS under allocations 2021-A0110811108 and 2022-A0130811108 made by GENCI.

Supporting Information Available

Detailed structures and polarization are reported on-line:

References

(1) Liu, Y.; Wang, Z.; Lin, C.; Zhang, J.; Feng, J.; Hou, B.; Yan, W.; Li, M.; Ren, Z. Spontaneous polarization of ferroelectric heterostructured nanorod arrays for high-performance photoelectrochemical cathodic protection. *App. Surf. Sc.* **2023**, *609*, 155345.

(2) Li, D.; Jiang, W.; Hao, H.; Wang, J.; Guo, Q.; Zhang, L.; Yao, Z.; Cao, M.; Liu, H. Amorphous/Crystalline Engineering of $BaTiO_3$-Based Thin Films for Energy-Storage Capacitors. *ACS Sustainable Chem. Eng.* **2022**, *10*, 1731–1740.

(3) Scott, J. Applications of modern ferroelectrics. *Science* **2007**, *315*, 954–959.

(4) Ju, L.; Tang, X.; Kou, L. Polarization boosted catalysis: progress and outlook. *Microstructures* **2022**, *2*, 2022008/1–2022008/17.

(5) Parravano, G. Ferroelectric Transitions and Heterogenous Catalysis. *J. Chem. Phys.* **1952**, *20*, 342.

(6) Inoue, Y.; Sato, K.; Hayashi, O. Adsorptive properties of semiconducting thin NiO and TiO_2 films combined with an oppositely polarized ferreoelectric support. *J. Chem. Soc., Faraday Trans. 1* **1987**, *83*, 3061–3068.

(7) Yun, Y.; Altman, E. Using Ferroelectric Poling to Change Adsorption on Oxide Surfaces. *J. Am. Chem. Soc.* **2007**, *129*, 15684–15689.

(8) Yun, Y.; Kampschulte, L.; Li, M.; Liao, D.; Altman, E. Effect of Ferroelectric Poling on the Adsorption of 2-Propanol on $LiNbO_3$(0001). *J. Phys. Chem. C* **2007**, *111*, 13951–13956.

(9) Kolpak, A.; Grinberg, I.; Rappe, A. Polarization Effects on the Surface Chemistry of $PbTiO_3$- Supported Pt films. *Phys. Rev. Lett.* **2007**, *98*, 166101/1–166101/4.

(10) Li, D.; Zhao, M.; Garra, J.; Kolpak, A.; Rappe, A.; Bonnell, D.; Vohs, J. Direct in situ determination of the polarization dependence of physisorption on ferroelectric surfaces. *Nature Mat.* **2008**, *7*, 473–477.

(11) Garra, J.; Vohs, J.; Bonnell, D. The effect of ferroelectric polarization on the interaction of water and methanol with the surface of $LiNbO_3$(0001). *Surf. Sci.* **2009**, *603*, 1106–1114.

(12) Yun, Y.; Pilet, N.; Schwarz, U.; Altman, E. Comparison of the interaction of Pd with positively and negatively poled $LiNbO_3$(0001). *Surf. Sci.* **2009**, *603*, 3145–3154.

(13) Garrity, K.; Kakekhani, A.; Kolpak, A.; Ismail-Beigi, S. Ferroelectric surface chemistry: First-principles study of $PbTiO_3$ surface. *Phys. Rev. B* **2013**, *88*, 045401–1–045401–11.

(14) Zhao, M.; Bonnell, D.; Vohs, J. Effect of ferroelectric polarization on the adsorption and reaction of ethanol on $BaTiO_3$. *Surf. Sci.* **2008**, *602*, 2849–2855.

(15) Zhao, M.; Bonnell, D.; Vohs, J. Influence of ferroelectric polarization on the energetics of the reaction of 2-fluoroethanol on $BaTiO_3$. *Surf. Sci.* **2009**, *603*, 284–290.

(16) Wang, R.; Fong, D.; Jiang, F.; Highland, M.; P.H.Fuoss,; Thompson, C.; Kolpak, A.; Eastman, J.; Streiffer, S.; Rappe, A.; Stephenson, G. Reversible Chemical Switching of a Ferroelectric Film. *Phys. Rev. Lett.* **2009**, *102*, 047601/1–047601/4.

(17) Deleuze, P.; Domenichini, B.; Dupont, C. Ferroelectric polarization switching induced from water adsorption in $BaTiO_3$ ultrathin films. *Phys. Rev. B* **2020**, *101*, 075410/1–075410/9.

(18) Kakekhani, A.; Ismail-Beigi, S. Ferroelectric-Based Catalysis: Switchable Surface Chemistry. *ACS Catal.* **2015**, *5*, 4537–4545.

(19) Kakekhani, A.; Ismail-Beigi, S. Polarization-driven catalysis *via* ferroelectric surfaces. *Phys. Chem. Chem. Phys.* **2016**, *18*, 19676–19695.

(20) Kakekhani, A.; Ismail-Beigi, S.; Altman, E. Ferroelectrics: A pathway to switchable chemistry and catalysis. *Surf. Sci.* **2016**, *650*, 302–316.

(21) Kakekhani, A.; Ismail-Beigi, S. Ferroelectric oxide surface chemistry: water splitting *via* pyroelectricity. *J. Mater. Chem. A* **2016**, *4*, 5235–5246.

(22) Alawode, B.; Kolpak, A. $PbTiO_3$(001) Capped with ZnO(1102): An ab Initio Study of the Effect of Substrate Polarization on Interface Composition and CO_2 dissociation. *J. Phys. Chem. Lett.* **2016**, *7*, 1310–1314.

(23) Nassreddine, S.; Morfin, F.; Niu, G.; Vilquin, B.; Gaillard, F.; Piccolo, L. Application of a sensitive catalytic reactor to the study of CO oxidation over $SrTiO_3$(100) and $BaTiO_3$/$SrTiO_3$(100) ferroelectric surfaces. *Surf. Interface Anal.* **2014**, *46*, 721–725.

(24) Rioult, M.; Datta, S.; Stanescu, D.; Stanescu, S.; Belkhou, R.; Maccherozzi, F.; Magnan, H.; Barbier, A. Tailoring the photocurrent in $BaTiO_3$/Nb:$SrTiO_3$ photoanodes by controlled ferroelectric polarization. *App. Phys. Lett.* **2015**, *107*, 103901/1–103901/4.

(25) Abbasi, P.; Barone, M.; de la Paz Cruz-Jàuregui, M.; Valdespino-Padilla, D.; Paik, H.; Kim, T.; Kornblum, L.; Schlom, D.; Pascal, T.; Fenning, D. Ferroelectric Modulation of Surface Electronic States in $BaTiO_3$ for Enhanced Hydrogen Evolution Reaction. *Nano Lett.* **2022**, *22*, 4276–4284.

(26) Kresse, G.; Furthmüller, J. Efficiency of ab-initio total energy calculations for metals and semiconductors using a plane-wave basis set. *Comput. Mater. Sci.* **1996**, *6*, 15 – 50.

(27) Kresse, G.; Furthmüller, J. Efficient iterative schemes for ab initio total-energy calculations using a plane-wave basis set. *Phys. Rev. B* **1996**, *54*, 11169–11186.

(28) Blöch, P. Projector augmented-wave method. *Phys. Rev. B* **1994**, *50*, 17953–17979.

(29) Kresse, G.; Joubert, D. From Ultrasoft Pseudopotentials to the Projector Augmented-Wave Method. *Phys. Rev. B* **1999**, *59*, 1758–1775.

(30) Perdew, J.; Burke, K.; Ernzerhof, M. Generalized Gradient Approximation Made Simple. *Phys. Rev. Lett.* **1996**, *77*, 3865–3868.

(31) Dudarev, S. L.; Botton, G. A.; Savrasov, S. Y.; Humphreys, C. J.; Sutton, A. P. Electron-Energy-Loss Spectra and the Structural Stability of Nickel Oxide: An LSDA+U study. *Phys. Rev. B* **1998**, *57*, 1505–1509.

(32) Deleuze, P.; Mahmoud, A.; Domenichini, B.; Dupont, C. Theoretical investigation of the platinum substrate influence on $BaTiO_3$ thin film polarisation. *Phys. Chem. Chem. Phys.* **2019**, *21*, 4367–4374.

(33) Sepliarsky, M.; Stachiotti, M.; Migoni, R. Interface Effects in Ferroelectric $PbTiO_3$ Ultrathin Films on a Paraelectric Substrate. *Phys. Rev. Lett.* **2006**, *96*, 137603/1–137603/4.

(34) Henkelman, G.; Uberuaga, B.; Jonsson, H. A climbing image nudged elastic band method for finding saddle points and minimum energy paths. *J. Chem. Phys.* **2000**, *113*, 9901–9904.

(35) Zhong, W.; King-Smith, R.; Vanderbilt, D. Giant LO-TO splittings in perovskite ferroelectrics. *Phys. Rev. Lett.* **1994**, *72*, 3618–3622.

(36) Shimada, T.; Tomoda, S.; Kitamura, T. *Ab initio* study of ferroelectric closure domains in ultrathin $PbTiO_3$ films. *Phys. Rev. B* **2010**, *81*, 144116/1–144116/6.

(37) Sauer, J.; Ugliengo, P.; Garrone, E.; Saunders, V. Theoretical Study of van der Waals Complexes at Surface Sites in Comparison with Experiments. *Chem. Rev.* **1994**, *94*, 2095–2160.

(38) Schlexer, P.; Widmann, D.; Behm, R. J.; Pacchioni, G. CO oxidation on a Au/TiO_2 Nanoparticle Catalyst via the Au-Assisted Mars-van Krevelen Mechanism. *ACS Catal.* **2018**, *8*, 6513–6525.

(39) Thang, H.; Pacchioni, G. CO Oxidation Promoted by a Pt_4/TiO_2 Catalyst: Role of Lattice Oxygen at the Metal/Oxide Interface. *Catal. Lett.* **2019**, *149*, 390–398.

(40) Cui, X.; Liu, J.; Yan, X.; Yang, Y.; Xiong, B. Exploring reaction mechanism of CO oxidation over $SrCoO_3$ catalyst: a DFT study. *App. Surf. Sc.* **2021**, *570*, 151234/1–151234/7.

(41) Datta, S.; Rioult, M.; Stanescu, D.; Magnan, H.; Barbier, A. Manipulating the ferroelectric polarization state of $BaTiO_3$ thin films. *Thin Solid Films* **2016**, *607*, 7–13.

TOC Graphic